^{7}Li + ^{11}B elastic and inelastic scattering in a coupled-reaction-channels approach

A. A. Rudchik,[1] A. T. Rudchik,[1] G. M. Kozeratska,[1] O. A. Ponkratenko,[1] E. I. Koshchy,[2] A. Budzanowski,[3] B. Czech,[3] S. Kliczewski,[3] R. Siudak,[3] I. Skwirczyńska, A. Szczurek,[3,4,*] S. Yu. Mezhevych,[1,5] K. W. Kemper,[6] J. Choiński,[7] T. Czosnyka,[7] and L. Głowacka[8]

[1]*Institute for Nuclear Research, Prospect Nauki 47, 03680 Kiev, Ukraine*
[2]*Kharkiv National University, ploshcha Svobody 4, 61077 Kharkiv, Ukraine*
[3]*H. Niewodniczański Institute of Nuclear Physics, Polish Academy of Sciences, ulitsa Radzikowskiego 152, PL-31-342 Cracow, Poland*
[4]*University of Rzeszów, PL-35-959 Rzeszów, Poland*
[5]*A. Sołtan Institute for Nuclear Studies, ulitsa Hoża 69, PL-00-681 Warsaw, Poland*
[6]*Physics Department, Florida State University, Tallahassee, Florida 32306-4350, USA*
[7]*Heavy Ion Laboratory, Warsaw University, ulitsa L. Pasteura 5A, PL-02-093 Warsaw, Poland*
[8]*Institute of Applied Physics, Military University of Technics, ulitsa Kaliskiego 2, PL-00-908 Warsaw, Poland*

(Received 5 March 2005; published 27 September 2005)

Angular distributions of ^{7}Li + ^{11}B elastic and inelastic scattering were measured at $E_{\rm lab}(^{11}{\rm B}) = 44$ MeV for the transitions to the ground and excited states of ^{7}Li and ^{11}B. The present data and data taken from the literature at $E_{\rm lab}(^{7}{\rm Li}) = 34$ MeV were analyzed within the optical model and coupled-reaction-channels methods. Elastic and inelastic scattering, reorientations of ^{7}Li and ^{11}B, and the most important one- and two-step transfers were included in the channels-coupling scheme. The dependence of the ^{7}Li + ^{11}B optical potential on kinetic energy was taken into account. The deformation parameters of ^{7}Li and ^{11}B and optical model parameters for interaction of these nuclei in ground and excited states were deduced. The contributions of one- and two-step transfers to the elastic and inelastic scattering were estimated.

DOI: 10.1103/PhysRevC.72.034608 PACS number(s): 25.70.Bc, 24.10.Eq, 24.10.Ht, 25.70.Hi

I. INTRODUCTION

At present there is tremendous interest in exploring the nuclear interactions of short-lived exotic nuclei. Some possible information can be gleaned from the scattering of stable nuclei with similar ground-state properties by analysis of the data with the coupled-channels method. For example, one can use ^{7}Li + ^{11}B collisions to learn about ^{8}Be + ^{10}B, and ^{6}Li + ^{12}B scattering by observing them as exit channels. One important question in these light nuclear systems is the energy dependence of the interaction parameters obtained from elastic- and inelastic-scattering data. Both ^{7}Li and ^{11}B have large ground-state quadrupole moments, and their influence on derived scattering potentials is important to understand, but because only one data set [1,2] existed for this system in the past it is possible to obtain results from a detailed analysis of it that are not general.

This work reports the elastic and inelastic scattering of ^{7}Li + ^{11}B taken at a bombarding energy of 44 MeV and the new data along with previously measured data at 34 MeV [1,2] were analyzed within the optical model (OM) and coupled-reaction-channels (CRC) methods [3]. Included in the CRC calculations were the ground-state reorientations of both nuclei as well as the important one- and two-step particle transfers. The CRC calculation involved modifications to the OM parameters for the excited nuclear states needed to describe the data, which allowed the difference between OM potentials for the ground and excited nuclear states to be studied. The existence of large-angle data in both data sets is crucial to determining the contributions of other processes to the measured elastic- and inelastic-scattering angular distributions.

The paper is organized as follows. Section II describes the experimental procedure and results, and Sec. III presents the OM and CRC calculations. The summary and conclusions are found in Sec. IV.

II. EXPERIMENTAL PROCEDURE

Angular distributions for the ^{7}Li(^{11}B,X) reactions were measured at the energy $E_{\rm lab}(^{11}{\rm B}) = 44$ MeV by use of a ^{11}B beam from the Warsaw University cyclotron C-200P. The energy spread of the exit cyclotron beam was about 1%. This spread was decreased to about 0.5% on target by a 3-mm collimator after the beam was rotated $\sim 30^{\circ}$ to the reaction chamber by a magnetic system.

A self-supporting 500-μg/cm^2 foil of natural lithium (92.5% of ^{7}Li) was used as a target. The reaction products were detected by a three-layer telescope consisting of an ionization chamber (ΔE_1 detector) and 0.5-mm ($E_1 = \Delta E_2$) and 2-mm (E_2) silicon detectors. The spectrometer was positioned with an accuracy of about 0.3°. The angular resolution in the lab system was $\sim 0.4^{\circ}$. Argon was used as a working gas in the ionization chamber at a pressure that was equivalent to ejectile energy losses that were the same as those in a 15-μm silicon detector. The heavy ($2 < Z < 8$) and light ($Z < 3$) ejectiles were detected by ΔE_1-E_1 and ΔE_2-E_2 telescopes, respectively. More details about the experimental setup are found in Ref. [4].

*Electronic address: Antoni.Szczurek@ifj.edu.pl

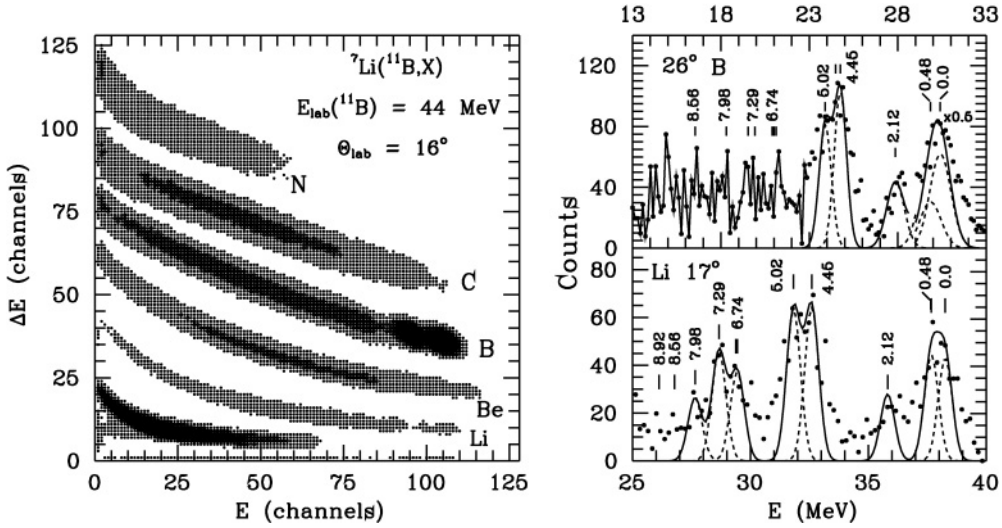

FIG. 1. Typical $\Delta E(E)$ (left-hand panel) and E spectra of boron and lithium isotopes (right-hand panel) ejected in the ^{7}Li(^{11}B, X) reactions at energy $E_{lab}(^{11}B) = 44$ MeV at angles of $\theta_{lab} = 16^\circ$, 26°, and 17°, respectively.

The standard CAMAC electronics and computer acquisition system SMAN [5] were used in the present experiment. The data were stored as $\Delta E_1(E_1)$ and $\Delta E_2(E_2)$ spectra.

A typical $\Delta E_1(E_1)$ spectrum is presented in Fig. 1 (left-hand panel). One can see that the individual elements were well resolved. Kinematic conditions were used to resolve isotope groups in the energy spectra obtained from corresponding two-dimensional spectra.

Figure 1 shows also typical energy spectra of boron (right-hand upper panel) and lithium (right-hand lower panel) isotopes. The given spectra are the residuals obtained by the subtraction of the continuous backgrounds from the measured spectra. The positions of the boron and lithium levels are indicated in the figures. The energy resolution limit of the experiment was about 0.4 MeV. The energy spectra were fitted by the sums of Gaussian symmetric functions by fixing the positions of peaks to the corresponding level kinetic energies, with a width obtained from well-isolated peaks observed in the $^{12}C + ^{11}B$ spectra measured in the given experiment. The fitting procedure of the energy spectra provided the areas under the poorly resolved peaks with errors of about 20−40%, which exceeded the statistical errors in most cases.

The resulting angular distributions of the elastic and inelastic scattering of $^7Li + ^{11}B$ are shown in Figs. 2–6. The angular distributions for the forward [$\theta^\circ_{c.m.}(^{11}B)$] and backward [$180^\circ - \theta^\circ_{c.m.}(^7Li)$] angles were obtained from the B and Li spectra, respectively, belonging to the same $\Delta E(E)$ spectrum at a given angle θ°_{lab}. Therefore the systematic errors of the forward and backward angle data are the same. The errors shown in Figs. 2–6 include the statistical errors and uncertainties of the spectrum fitting procedure. The angular distribution of the elastic scattering was normalized to the OM cross-section at small angles where the OM parameter uncertainties play only a minor role. The normalization error was smaller than 15%. The same factor was used to normalize the angular distributions for both elastic- and inelastic-scattering data at the forward and backward angles. The good agreement of the 7.978-MeV inelastic-scattering data (Fig. 5) obtained from the B and Li spectra in the overlap angle interval $\theta^\circ_{c.m.} \approx 100^\circ - 110^\circ$, is substantial evidence of reasonable normalization of the backward angle data.

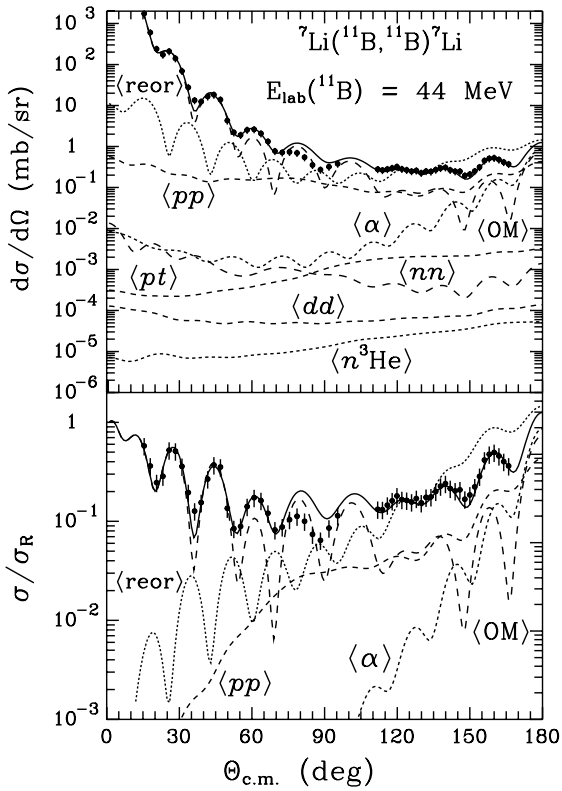

FIG. 2. Angular distributions of $^7Li + ^{11}B$ elastic scattering at $E_{lab}(^{11}B) = 44$ MeV. The curves show the OM and CRC angular distributions of the potential scattering (curves ⟨OM⟩), reorientations of ^{7}Li and ^{11}B (curves ⟨reor⟩) and transfers (other curves). The solid curves represent the coherent sums of these processes.

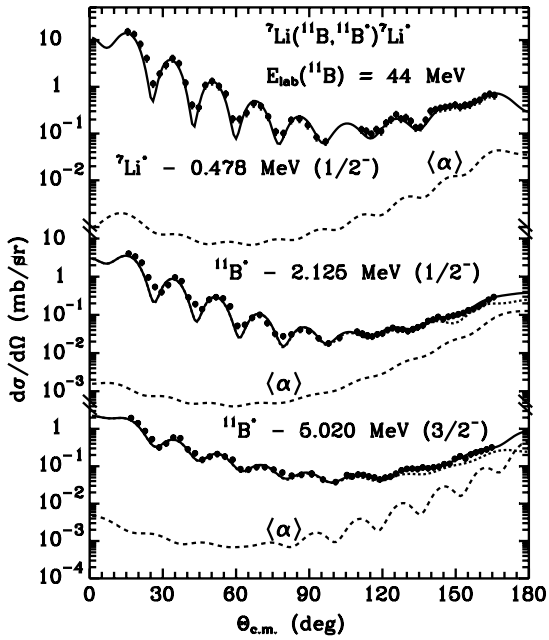

FIG. 3. Angular distributions of ^{7}Li + ^{11}B inelastic scattering at $E_{\rm lab}(^{11}{\rm B}) = 44$ MeV for the transition to the 0.478-MeV (1/2$^-$) state of ^{7}Li and 2.125-MeV (1/2$^-$) and 5.02-MeV (3/2$^-$) excited states of ^{11}B. The curves show the CRC angular distributions of collective nature excitations (dotted curves) and α-cluster transfers (curves $\langle\alpha\rangle$). Solid curves represent the coherent sums of these processes.

The data at 34 MeV [1,2] analyzed in this work were taken without errors from the figures of corresponding articles.

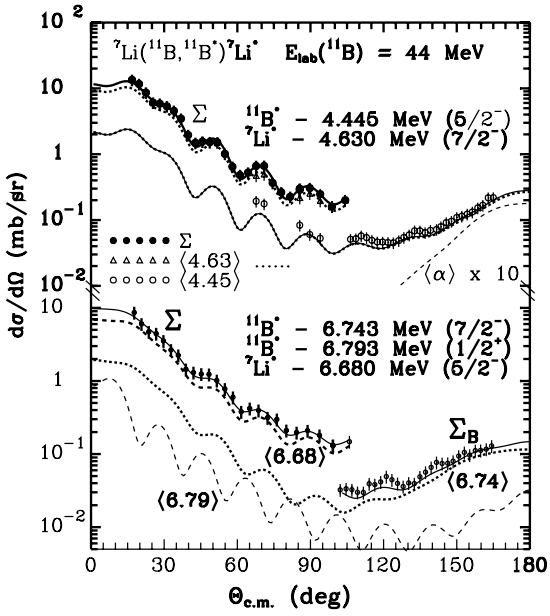

FIG. 4. The same as in Fig. 3 but for the 4.63-MeV (7/2$^-$) and 6.68-MeV (5/2$^-$) excited states of ^{7}Li and the 4.445-MeV (5/2$^-$), 6.743-MeV (7/2$^-$), and 6.793-MeV (1/2$^+$) excited states of ^{11}B. Curves Σ and Σ_B show the incoherent sums of these transitions.

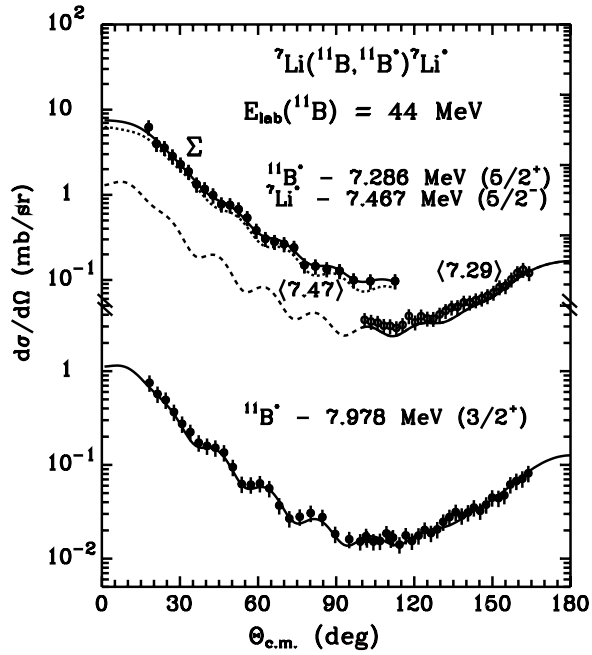

FIG. 5. The same as in Fig. 3 but for the 7.467-MeV (5/2$^-$) excited state of ^{7}Li and the 7.286-MeV (5/2$^+$), and 7.978-MeV (3/2$^+$) excited states of ^{11}B.

III. DATA ANALYSIS

A. OM and CRC calculation procedures

OM potentials of the Woods-Saxon type;

$$U(r) = V_0 f(r, R_V, a_V) + i W_S f(r, R_W, a_W), \qquad (1)$$

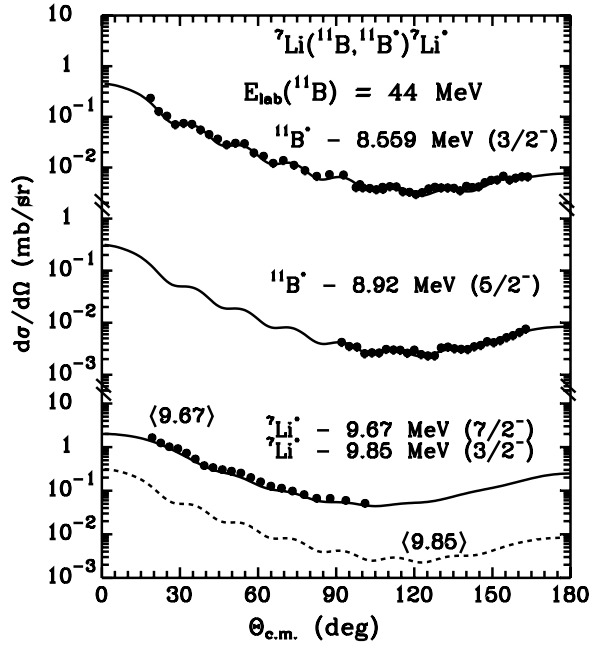

FIG. 6. The same as in Fig. 3 but for the 9.67-MeV (7/2$^-$) and 9.85-MeV (3/2$^-$) excited states of ^{7}Li and the 8.559-MeV (3/2$^-$) and 8.92-MeV (5/2$^-$) excited states of ^{11}B.

and Coulomb potentials of uniform charged sphere,

$$VC(r) = \begin{cases} \frac{Z_P Z_T e^2}{2R_C}\left(3 - \frac{r^2}{R_C^2}\right), & r \leqslant R_C \\ \frac{Z_P Z_T e^2}{r}, & r > R_C, \end{cases} \quad (2)$$

were used in the OM and CRC calculations for both entrance and exit channels of the $^7\mathrm{Li} + ^{11}\mathrm{B}$ elastic and inelastic scattering. The preceding radial functions are given by

$$f(r, R_i, a_i) = \left[1 + \exp\left(\frac{r - R_i}{a_i}\right)\right]^{-1}, \quad (3)$$

$$R_i = r_i\left(A_P^{1/3} + A_T^{1/3}\right), i = V, W, C, \quad (4)$$

where Z_P, Z_T and A_P, A_T are the charges and masses of the projectile and target, respectively.

The radius of the Coulomb potential for the entrance and exit channels was fixed at the value of $r_C = 1.25$ fm. The OM parameters $X = \{X_i\} = \{V_0, r_V, a_V, W_S, r_W, a_W\}$ were fitted within the OM to obtain a good description of the elastic-scattering data for $\theta_{\mathrm{c.m.}} < 90^\circ$. The optimal set X_{opt} of the OM parameters deduced was used as the initial one in the CRC calculations. For the elastic-scattering channel, only the parameter W_S was fitted in these calculations. All OM parameters X_i for the exit inelastic-scattering channels were fitted because these OM parameters can differ from those of the elastic-scattering channel because of the strong dependence of the OM parameters on the kinetic energy of the ejectiles in the excited states, their structure (parameters a_i), and absorption properties (W_S).

In the fitting procedure, the Pauli principle was taken into account by use of the radius R_{comp} of the compound nucleus $A_P + A_T$ for the lower limit of parameter R_V:

$$R_{\mathrm{comp}} \approx 1.25(A_P + A_T)^{1/3} \leqslant R_V = r_V\left(A_P^{1/3} + A_T^{1/3}\right) \quad (5)$$

and

$$r_V \geqslant 1.25(A_P + A_T)^{1/3} \Big/ \left(A_P^{1/3} + A_T^{1/3}\right). \quad (6)$$

For the $^7\mathrm{Li} + ^{11}\mathrm{B}$ scattering, $r_V \geqslant 0.792$ fm.

The parameter a_W was limited by the relation $a_W \leqslant a_V$ to guarantee that always

$$W(r) = W_S f(r, R_W, a_W) \leqslant V(r) = V_0 f(r, R_V, a_V). \quad (7)$$

This limit means that the inelastic nuclear processes cannot occur without corresponding elastic scattering. Consequently, we used only the parameters W_S, a_W, and r_W that fulfilled relation (7). The code SPI-GENOA [6] was used for the OM calculations.

In the CRC analysis, $^7\mathrm{Li} + ^{11}\mathrm{B}$ elastic and inelastic scattering for the transitions to the ground and excited states of ^{7}Li and ^{11}B (up to 9.85 MeV) as well as the most important transfer reactions were included in the coupled-channels scheme. Figure 7 shows the transitions to the excited states of ^{7}Li and ^{11}B. The reorientations of these nuclei in the excited states were also included in the CRC calculations. The diagrams of one- and two-step transfers, which contribute to the $^7\mathrm{Li} + ^{11}\mathrm{B}$ scattering, are presented in Fig. 8.

We assume that the rotations of the deformed ^{7}Li and ^{11}B nuclei and vibrations dominate in the low-energy excitations.

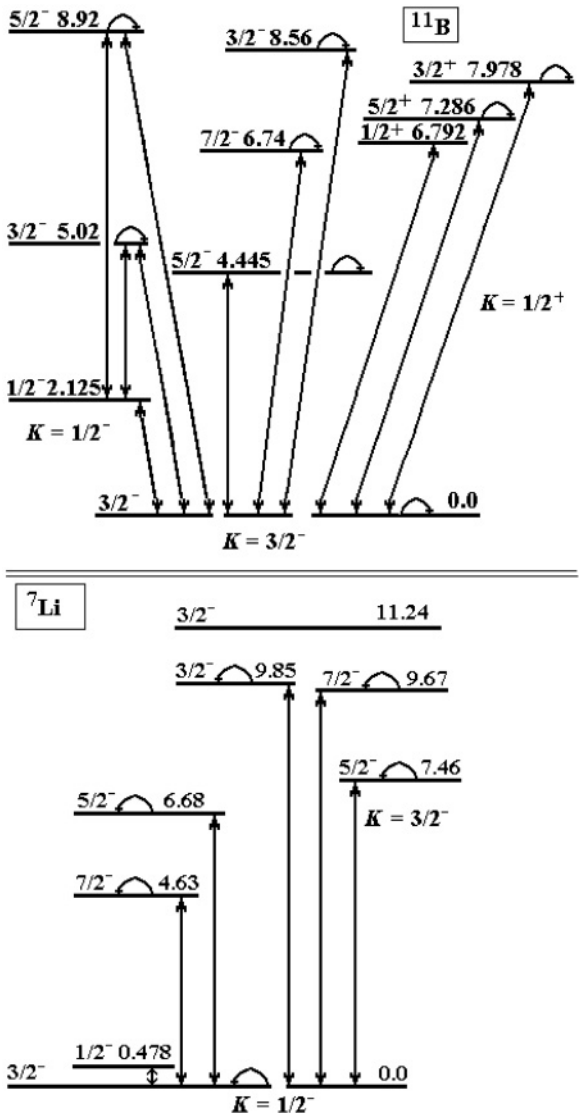

FIG. 7. Coupling schemes for the transitions to the excited states of ^{7}Li and ^{11}B.

The transitions to these states were calculated with the form factors

$$V_\lambda(r) = -\frac{\delta_\lambda}{\sqrt{4\pi}}\frac{dU(r)}{dr}, \quad (8)$$

where δ_λ is the length of the λ multipole deformation. The deformation parameters are listed in Table I.

Reorientation is considered as the quadrupole transition

$$\langle E, J^\pi | V_2 | E, J^\pi \rangle. \quad (9)$$

The spectroscopic amplitudes S_x of transferred clusters or nucleons x in the systems $A = C + x$ were calculated within the translationally invariant shell model (TISM) [8] with the code DESNA [9,10] and Boyarkina's wave-function tables [11]. The $\Psi_i = |N_i[f_i](\lambda_i\mu_i)\alpha_i L_i S_i J_i T_i\rangle$ $(i = A, C, x)$ oscillatory wave functions of SU(3) symmetry $(\lambda_i\mu_i)$ (orbital part) and SU(4) symmetry $[f_i]$ (spin-isospin part) were used in the

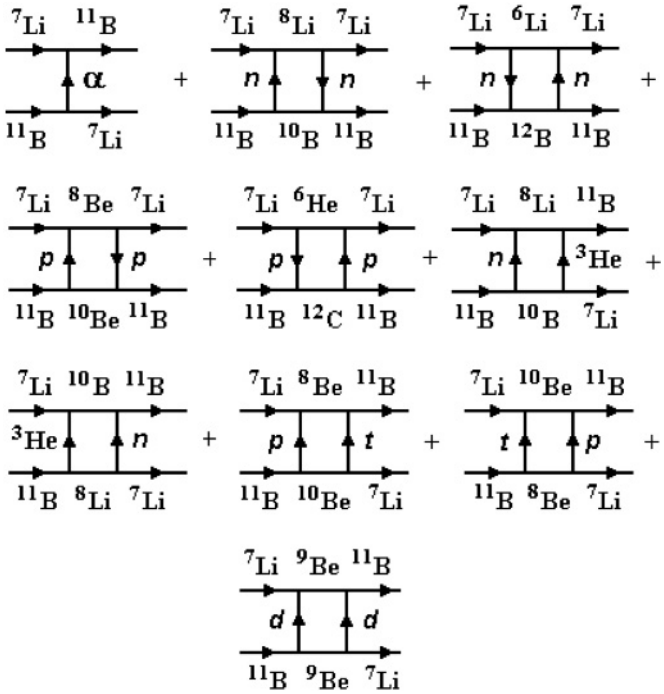

FIG. 8. Diagrams of one- and two-step transfers contributing to the ^{7}Li + ^{11}B elastic- and inelastic-scattering calculations.

calculations of the spectroscopic amplitudes,

$$S_x = \begin{pmatrix} A \\ x \end{pmatrix}^{1/2} \langle \Psi_A | \Psi_C \Psi_x ; \varphi_{Cx} \rangle,$$

where $[f_i]$ and T_i are Young tableau and isospins, respectively, α_i are other quantum numbers, $\boldsymbol{J_i} = \boldsymbol{L_i} + \boldsymbol{S_i}$. The wave function $\varphi_{Cx} = |nLj\rangle$ describes the $x + C$ relative motion. Amplitudes S_x are listed in Table II.

We calculated the bound-cluster wave function by fitting the Woods-Saxon potential parameter V to the x-cluster binding energy for $a = 0.65$ fm and $r_V = 1.25A^{1/3}/(C^{1/3} + x^{1/3})$ fm. The code FRESCO [3] was used in the CRC calculation.

B. Elastic scattering

First, the ^{7}Li + ^{11}B elastic-scattering data at the energies $E_{\rm lab}(^{11}{\rm B}) = 44$ MeV ($E_{\rm c.m.} = 17.11$ MeV) (this work) and $E_{\rm lab}(^7{\rm Li}) = 34$ MeV ($E_{\rm c.m.} = 20.78$ MeV [1,2]) were analyzed within the OM. The set of the OM parameters $X_i = V_0, r_V, a_V, W_S, r_W, a_W$ was fitted to the data for the angles $\theta_{\rm c.m.} < 90^\circ$. The corresponding OM angular distributions are shown in Figs. 2 and 9 (curves ⟨OM⟩). The OM greatly underpredicts the large-angle data.

Next, the obtained OM parameters $\{X_i\}$ were used as a start in the CRC fit. The CRC calculations were performed including elastic and inelastic scattering, reorientations of ^{7}Li and ^{11}B, and α-cluster and $p + p$ transfers in the coupling-channels scheme. The deduced OM parameters $\{X_i\}$ are listed in Table III.

Finally, the contributions of transfer reactions to the elastic-scattering data were calculated. They are shown in Figs. 2 and 9 by the curves marked ⟨process name⟩ (curves ⟨reor⟩ show the cross section of ^{7}Li and ^{11}B reorientations, curve ⟨pt⟩ corresponds to the coherent sum of $p + t$ and $t + p$ transfers, and so on). One can see that the contribution of most transfer reactions to the elastic scattering are negligible. Only the α-cluster and sequential $p + p$ transfers (curves ⟨α⟩ and ⟨pp⟩, respectively) give small contributions to the data at large angles. Figures 2 and 9 show that the reorientations of ^{7}Li and ^{11}B (curves ⟨reor⟩) cause mostly the large-angle enhancement of the elastic scattering. The coherent sums of the potential scattering, reorientations, and transfers of α and $p + p$ (solid curves) describe the ^{7}Li + ^{11}B elastic-scattering data quite satisfactorily.

TABLE I. Deformation parameters of ^{7}Li and ^{11}B (β_λ for $R = 1.25A^{1/3}$ fm).

Nuclei	E_x (MeV)	J^π	λ	δ_λ (fm)	β_λ	Ref.
^{7}Li	0.0	$3/2^-$	2	2.0	0.84	[2]
	0.478	$1/2^-$	2	2.0	0.84	[2]
	4.630	$7/2^-$	2	2.0	0.84	
			4	1.0	0.42	
	6.680	$5/2^-$	2	2.0	0.84	
			4	1.0	0.42	
	7.460	$5/2^-$	2	2.0	0.84	
			4	1.0	0.42	
	9.670	$7/2^-$	2	2.0	0.84	
			4	1.0	0.42	
	9.850	$3/2^-$	2	2.0	0.84	
^{11}B	2.125	$1/2^-$	2	1.2	0.43	[7]
	4.445	$5/2^-$	2	1.2	0.43	[7]
			4	1.0	0.36	[7]
	5.020	$3/2^-$	2	1.2	0.43	[7]
	6.743	$7/2^-$	2	1.2	0.43	[7]
			4	1.0	0.36	[7]
	6.792	$1/2^+$	1	1.0	0.36	[7]
	7.286	$5/2^+$	1	1.0	0.36	[7]
			3	1.2	0.43	[7]
	7.978	$3/2^+$	1	1.0	0.36	[7]
			3	1.2	0.43	[7]
	8.560	$3/2^-$	2	1.8	0.65	[7]
	8.920	$5/2^-$	2	1.2	0.43	
			4	1.0	0.36	

C. Inelastic scattering

The angular distributions of ^{7}Li + ^{11}B inelastic scattering at $E_{\rm lab}(^{11}{\rm B}) = 44$ MeV and at $E_{\rm lab}(^7{\rm Li}) = 34$ MeV [1,2] are shown in Figs. 3−6 and Figs. 9 and 10, respectively. The curves represent the CRC cross sections calculated with the deformation and OM parameters listed in Tables I and III, respectively. The OM parameters for the ^{7}Li*+^{11}B and ^{7}Li + ^{11}B* exit channels were fitted to the inelastic-scattering data. As in the previous case, the contributions of the transfer reactions to the data were estimated. It was found that they are negligible (curves ⟨α⟩ and ⟨pp⟩ in Figs. 3−6, 9, and 10). The reorientations of ^{7}Li and ^{11}B in excited states were found to give small contributions to the data.

TABLE II. Spectroscopic amplitudes S_x of x clusters in the $A = C + x$ systems.

A	C	x	nL_j	S_x
^{7}Li	^{6}He	p	$1P_{3/2}$	0.805
^{7}Li$^{*}_{0.478}$	^{6}He	p	$1P_{1/2}$	0.805
^{7}Li	^{6}Li	n	$1P_{1/2}$	−0.657
			$1P_{3/2}$	−0.735[a]
^{8}Li	^{7}Li	n	$1P_{1/2}$	0.478
^{8}Be	^{7}Li	p	$1P_{3/2}$	1.234[a]
^{8}Be	^{7}Li$^{*}_{0.478}$	p	$1P_{1/2}$	0.873[a]
^{9}Be	^{7}Li	d	$2S_1$	−0.226[a]
			$1D_1$	0.111[a]
			$1D_3$	−0.624[a]
^{10}Be	^{7}Li	t	$2P_{3/2}$	0.392[a]
^{10}B	^{7}Li	^{3}He	$1P_{3/2}$	0.419
			$1F_{5/2}$	−0.104[a]
			$1F_{7/2}$	0.347
^{11}B	^{7}Li	α	$3S_0$	−0.638
			$2D_2$	−0.422
^{11}B	^{7}Li$^{*}_{0.478}$	α	$2D_2$	−0.422[a]
^{11}B	^{7}Li$^{*}_{4.63}$	α	$2D_2$	0.362
			$1G_4$	0.429
^{11}B	^{7}Li$^{*}_{6.68}$	α	$2D_2$	0.148[a]
			$1G_4$	0.575[a]
^{11}B	^{7}Li$^{*}_{9.67}$	α	$2D_2$	0.362
			$1G_4$	0.429
^{11}B	^{7}Li$^{*}_{9.85}$	α	$3S_0$	−0.638
			$2D_2$	−0.422
^{11}B$^{*}_{2.125}$	^{7}Li	α	$2D_2$	0.596[a]
^{11}B$^{*}_{4.445}$	^{7}Li	α	$2D_2$	−0.049[a]
			$1G_4$	−0.192[a]
^{11}B$^{*}_{5.020}$	^{7}Li	α	$3S_0$	−0.638
			$2D_2$	−0.422
^{11}B$^{*}_{6.743}$	^{7}Li	α	$2D_2$	0.104
			$1G_4$	0.124
^{11}B$^{*}_{6.793}$	^{7}Li	α	$2D_2$	0.596[a]
^{11}B$^{*}_{7.286}$	^{7}Li	α	$2D_2$	−0.049[a]
			$1G_4$	−0.192[a]
^{11}B	^{8}Li	^{3}He	$1P_{1/2}$	0.160[a]
			$1F_{5/2}$	0.218[a]
			$1F_{7/2}$	0.214
^{11}B	^{8}Be	t	$2P_{3/2}$	0.641
^{11}B	^{9}Be	d	$2S_1$	−0.607[a]
			$1D_1$	−0.109[a]
			$1D_3$	0.610[a]
^{11}B	^{10}Be	p	$1P_{3/2}$	0.699
^{11}B$^{*}_{2.125}$	^{10}Be	p	$1P_{1/2}$	0.699
^{11}B	^{10}B	n	$1P_{3/2}$	−1.347[a]
^{12}B	^{11}B	n	$1P_{1/2}$	−0.142[a]
			$1P_{3/2}$	−0.127
^{12}C	^{11}B	p	$1P_{3/2}$	−1.706[a]
^{12}C	^{11}B$^{*}_{2.125}$	p	$1P_{1/2}$	−1.206[a]
^{12}C	^{11}B$^{*}_{5.021}$	p	$1P_{3/2}$	−1.706[a]
^{12}C	^{11}B$^{*}_{6.793}$	p	$1P_{1/2}$	−1.206[a]

[a] $S_{\mathrm{FRESCO}} = (-1)^{J_C+j-J_A} S_x = -S_x$.

The large-angle scattering data for the 0.478-MeV transition at 34 MeV are purely described by the CRC angular distribution (lower panel in Fig. 9). The set A of OM parameters provides a satisfactory description of the data only to $\theta_{\mathrm{c.m.}} \approx 140^{\circ}$. By increasing the absorption potential, it is possible to improve the description of the large-angle data (set B) at the cost of worsening the middle-angle fit. More large-angle data would allow a more detailed study of the physics affecting the large-angle scattering.

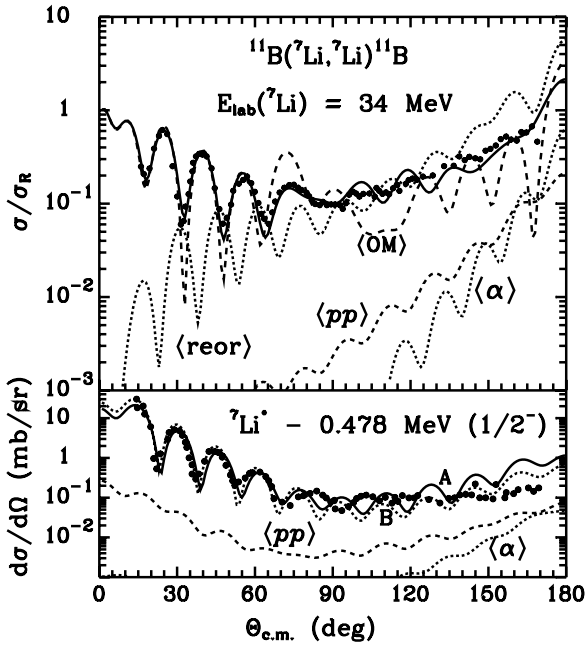

FIG. 9. Angular distributions of ^{7}Li + ^{11}B scattering at the energy $E_{\mathrm{lab}}(^{7}\mathrm{Li}) = 34$ MeV [2] for the transitions to the ground states of these nuclei (upper panel) and 0.478 MeV ($1/2^{-}$) state of ^{7}Li (lower panel). The curves are the same as those in Fig. 2 but for the energy $E_{\mathrm{lab}}(^{7}\mathrm{Li}) = 34$ MeV.

The transitions to the 4.445-MeV ($5/2^{-}$) state of ^{11}B and the 4.63-MeV ($7/2^{-}$) state of ^{7}Li to the 6.743-MeV ($7/2^{-}$) and 6.793-MeV ($1/2^{+}$) states of ^{11}B and the 6.68-MeV ($5/2^{-}$) state of ^{7}Li (Fig. 4) as well as to the 7.286-MeV ($5/2^{+}$) state of ^{11}B and 7.467-MeV ($5/2^{-}$) state of ^{7}Li (Fig. 5) were unresolved in the experiment at forward hemisphere angles. As one can see, the transitions to the excited states of ^{7}Li dominate in both these cases. The solid curves Σ and Σ_B show incoherent sums of the unresolved states. The CRC angular distributions describe the data satisfactorily.

Figure 6 shows that the transition to the 9.67-MeV ($7/2^{-}$) excited state of ^{7}Li dominates the data for the unresolved 9.67 MeV ($7/2^{-}$) + 9.85 MeV ($3/2^{-}$) states of ^{7}Li.

D. OM parameters for the excited nuclei

As was mentioned in the preceding subsection, the OM parameters for the excited ^{7}Li and ^{11}B nuclei were fitted to the inelastic-scattering data to take into account the energy dependence of these parameters and possible differences between an interaction of nuclei in their ground and excited states. The obtained OM parameter sets $\{X_i\} = \{V, W_S, r_V, r_W, a_V, a_W\}$ for the excited ^{7}Li and ^{11}B are given in Table III and shown in Fig. 11. It is most striking that the

TABLE III. Parameters of the Woods-Saxon OM potentials.

Channels	$E_{\text{c.m.}}$ (MeV)	V_0 (MeV)	r_V (fm)	a_V (fm)	W_s (MeV)	r_W (fm)	a_W (fm)
$^{7}\text{Li}^{*}_{9.85} + ^{11}\text{B}$	7.26	90.5	0.874	0.580	7.1	1.370	0.533
	10.93	138.5	0.815	0.614	7.7	1.288	0.574
$^{7}\text{Li}^{*}_{9.67} + ^{11}\text{B}$	7.44	92.3	0.872	0.581	7.1	1.367	0.535
	11.11	140.9	0.813	0.616	7.8	1.284	0.576
$^{7}\text{Li} + ^{11}\text{B}^{*}_{8.92}$	8.19	100.5	0.860	0.587	7.2	1.350	0.542
	11.86	150.6	0.806	0.624	8.0	1.274	0.586
$^{7}\text{Li} + ^{11}\text{B}^{*}_{8.56}$	8.55	104.7	0.854	0.590	7.2	1.342	0.546
	12.22	154.9	0.803	0.628	8.2	1.270	0.590
$^{7}\text{Li} + ^{11}\text{B}^{*}_{7.98}$	9.13	111.8	0.844	0.596	7.3	1.327	0.552
	12.80	161.6	0.800	0.634	8.4	1.264	0.597
$^{7}\text{Li}^{*}_{7.47} + ^{11}\text{B}$	9.64	118.4	0.835	0.601	7.3	1.315	0.558
	13.31	167.1	0.798	0.639	8.7	1.261	0.603
$^{7}\text{Li} + ^{11}\text{B}^{*}_{7.29}$	9.83	120.8	0.832	0.602	6.4	1.310	0.560
	13.49	168.9	0.797	0.641	5.8	1.260	0.604
$^{7}\text{Li} + ^{11}\text{B}^{*}_{6.79}$	10.32	127.5	0.824	0.608	7.5	1.299	0.566
	13.98	173.6	0.796	0.645	9.0	1.257	0.609
$^{7}\text{Li} + ^{11}\text{B}^{*}_{6.74}$	10.37	128.2	0.823	0.608	7.5	1.298	0.567
	14.03	174.0	0.796	0.645	9.0	1.257	0.610
$^{7}\text{Li}^{*}_{6.68} + ^{11}\text{B}$	10.43	129.1	0.822	0.609	7.5	1.297	0.568
	14.10	174.6	0.795	0.646	9.1	1.257	0.611
$^{7}\text{Li} + ^{11}\text{B}^{*}_{5.02}$	12.09	152.2	0.804	0.627	6.2	1.270	0.588
	15.76	196.5	0.793	0.580	3.5	1.252	0.540
$^{7}\text{Li}^{*}_{4.63} + ^{11}\text{B}$	12.48	157.5	0.802	0.631	8.8	1.266	0.593
	16.15	188.3	0.793	0.660	10.0	1.252	0.627
$^{7}\text{Li} + ^{11}\text{B}^{*}_{4.45}$	12.67	159.8	0.801	0.633	8.9	1.265	0.595
	16.33	189.1	0.793	0.600	4.5	1.252	0.540
$^{7}\text{Li} + ^{11}\text{B}^{*}_{2.13}$	14.99	183.9	0.794	0.653	10.2	1.254	0.619
	18.65	189.4	0.792	0.671	10.7	1.250	0.639
$^{7}\text{Li}^{*}_{0.48} + ^{11}\text{B}$	16.63	188.2	0.792	0.663	11.0	1.251	0.630
A	20.30	189.2	0.792	0.674	11.5	1.250	0.644
B	20.30	189.2	0.792	0.675	13.0	1.350	0.644
$^{7}\text{Li} + ^{11}\text{B}$	17.11	188.0	0.792	0.665	11.0	1.251	0.633
	20.78	189.2	0.792	0.675	10.2	1.250	0.644

parameter W_S for the 4.445-MeV ($5/2^{-}$), 5.021-MeV ($3/2^{-}$), and 7.286-MeV ($5/2^{-}$) excited ^{11}B states is quite different from the average energy dependence of this parameter for other excited states of ^{11}B.

The energy dependence of the OM parameters was fitted by the forms [12]

$$X_i(E) = \begin{cases} X_i^{\max} - \left(X_i^{\max} - X_i^{\min}\right) g(E, E_{X_i}, \Delta E_{X_i}) \\ \qquad \text{for } X_i = V_0, W_S, a_v, a_w \\ X_i^{\min} + \left(X_i^{\max} - X_i^{\min}\right) g(E, E_{X_i}, \Delta E_{X_i}) \\ \qquad \text{for } X_i = r_v, r_w, \end{cases} \tag{10}$$

where

$$g(E, E_{X_i}, \Delta E_{X_i}) = \left[1 + \exp\left(\frac{E - E_{X_i}}{\Delta E_{X_i}}\right)\right]^{-1}, \tag{11}$$

$\{Y_i\} = \{ X_i^{\min}, X_i^{\max}, E_{X_i}, \Delta E_{X_i}\}$ are the energy dependence parameters $E = E_{\text{c.m.}}$. The parameters $X_i^{\min}$ and $X_i^{\max}$ define the lower and upper limits of the OM parameter X_i, respectively. The parameter E_{X_i} is the energy at which $X_i(E_{X_i}) = (X_i^{\max} - X_i^{\min})/2$.

In addition to the form of Eqs. (10) and (11), the dispersion relation between the real $V(r, E)$ and imaginary $W(r, E)$ parts of the OM potential was used [13]:

$$V(r, E) = V_0(r, E) + \Delta V_W(r, E), \tag{12}$$

where

$$\Delta V_W(r, E) = \frac{\mathbf{P}}{\pi} \int_0^{\infty} \frac{W(r, E')}{E' - E} dE', \tag{13}$$

and **P** denotes the principal value of the integral $\Delta V_W(r, E)$. At $r = 0$, Eqs. (12) and (13) express the relation between the parameters $V_0 \equiv V(0, E)$ and W_S of the Woods-Saxon potential (1).

The parameters $Y_i = X_i^{\min}, X_i^{\max}, E_{X_i}$, and ΔE_{X_i} were fitted to the OM parameters X_i given in Table III. As a result, the sets of the parameters $Y_i = X_i^{\min}, X_i^{\max}$, E_{X_i}, and ΔE_{X_i} were deduced for $^{7}\text{Li} + ^{11}\text{B}$ elastic and inelastic scattering. These parameters are listed in Table IV. The corresponding energy dependences of the OM parameters for the interaction of ^{7}Li and ^{11}B in their ground and excited states are presented in Fig. 11 by the curves marked by $V_0 \equiv V_0(0, E)$, $V \equiv V(0, E)$, and $\Delta V \equiv \Delta V_W(0, E)$.

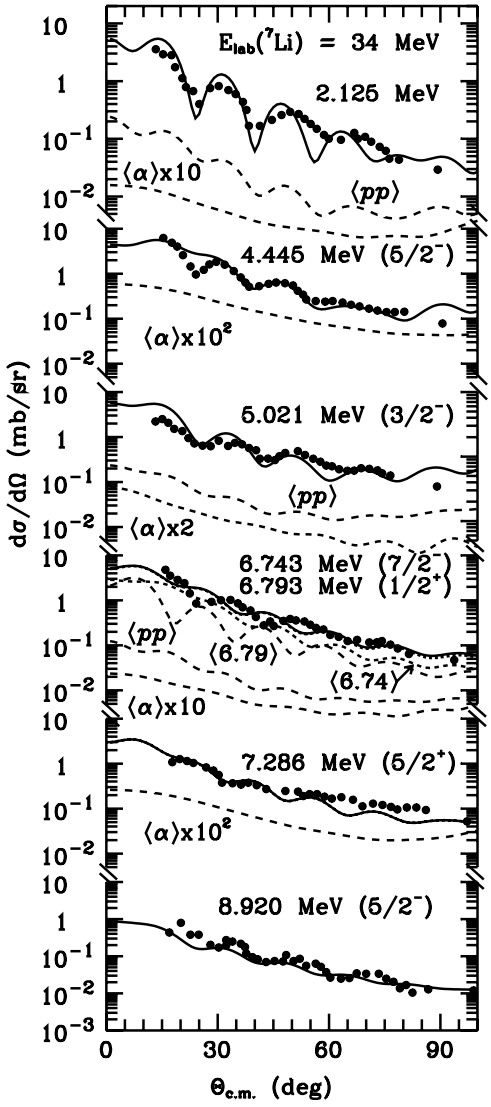

FIG. 10. The same as in Fig. 3 but for the excited states of ^{11}B at energy $E_{\rm lab}(^7{\rm Li}) = 34$ MeV [2].

In Fig. 11 we also present the energy dependence of $^7{\rm Li} + ^{14}{\rm N}$ OM parameters of $V \equiv V(0, E)$ and W_S (curves ^{14}N) [14]. One can see that the parameters for the $^7{\rm Li} + ^{14}{\rm N}$ interaction achieve their maxima at higher energies than in the case of $^7{\rm Li} + ^{11}{\rm B}$ scattering. This effect is due to the higher potential barrier for the first system. In the past, such effects were observed for ^{8}Be + ^{15}N and ^{8}Be + ^{13}C interactions [15].

TABLE IV. Energy dependence of the $^7{\rm Li} + ^{11}{\rm B}$ OM parameters.

X_i / Y_i	V_0 (MeV)	W_S (MeV)	r_V (fm)	r_W (fm)	a_V (fm)	a_W (fm)
$X_i^{\rm min}$	113.1	7.0	0.792	1.250	0.550	0.500
$X_i^{\rm max}$	307.0	10.9	0.899	1.412	0.680	0.650
E_{X_i}, MeV	11.7	13.6	9.044	8.970	11.000	11.000
Δ_{X_i}, MeV	3.1	1.6	1.490	1.633	3.000	3.000

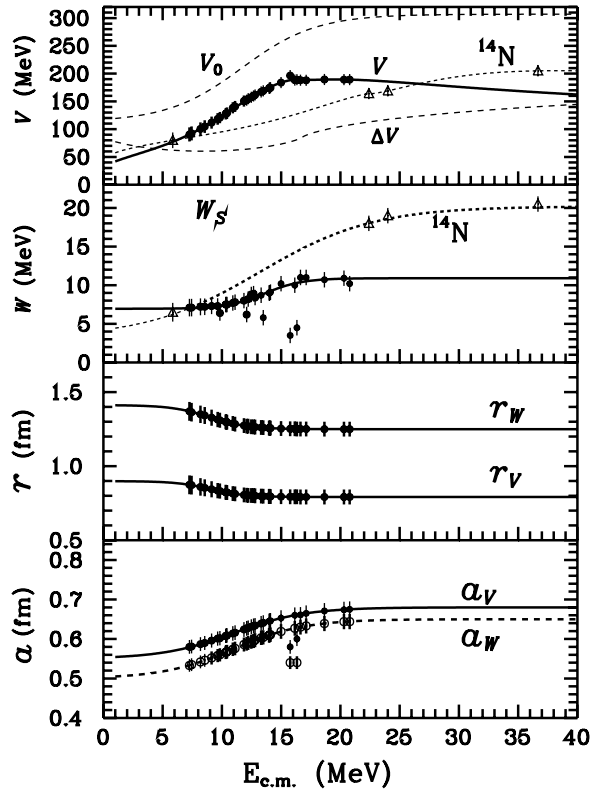

FIG. 11. Energy dependence of OM potential parameters for the interaction of ^{7}Li and ^{11}B in ground and excited states versus the same for the $^7{\rm Li} + ^{14}{\rm N}$ interaction (curves ^{14}N) [12]. Note that $V_0 \equiv V_0(0, E)$, $V \equiv V(0, E)$, $\Delta V \equiv \Delta V_W(0, E)$ according to Eq. (12).

IV. SUMMARY AND CONCLUSIONS

New data for the angular distributions of $^7{\rm Li} + ^{11}{\rm B}$ elastic and inelastic scattering at energy $E_{\rm lab}(^{11}{\rm B}) = 44$ MeV were measured for transitions to the ground states of these nuclei and to the excited states at energies $E(^7{\rm Li}^*) = 0.478$–9.85 MeV and $E(^{11}{\rm B}^*) = 2.125$–$8.92$ MeV. These data and the data for the $^7{\rm Li} + ^{11}{\rm B}$ elastic and inelastic scattering at energy $E_{\rm lab}(^7{\rm Li}) = 34$ MeV [1,2] were analyzed within the OM and CRC methods. The transitions to the excited states were calculated with the rotational model. Elastic and inelastic channels with reorientations of ^{7}Li and ^{11}B as well as the strong particle transfers were included in the coupling scheme.

In the $^7{\rm Li} + ^{11}{\rm B}$ elastic channel, the potential scattering and reorientations of ^{7}Li and ^{11}B dominate at forward and backward angles, respectively. The rotational transitions to the excited states of ^{7}Li and ^{11}B dominate the inelastic channels. The contributions of one- and two-step transfers to the elastic and inelastic channels are small. The α-cluster and sequential proton + proton transfers dominates the transfer channels.

As a result, the $^7{\rm Li} + ^{11}{\rm B}$ OM parameters for the ground and excited states of ^{7}Li and ^{11}B as well as deformation parameters of these nuclei were deduced. It was also found that the OM parameter W_S for the $^7{\rm Li} + ^{11}{\rm B}^*$ channels with the 4.445-MeV ($5/2^-$), 5.021-MeV ($3/2^-$), and 7.286-MeV ($5/2^-$) states of ^{11}B is smaller (weaker absorption) when compared with other states of these nuclei.

The energy dependence of the ^{7}Li + ^{11}B OM parameters for the ground and excited states of ^{7}Li and ^{11}B was obtained at energies $E_{\mathrm{c.m.}} \approx 7-21$ MeV. It was found that this energy dependence is different from that of the ^{7}Li + ^{14}N interaction [15].

ACKNOWLEDGMENTS

We thank A. Sobiczewski and J. Jastrzebski for their interest in this work. We are indebted to the technical staff of the Heavy Ion Laboratory of Warsaw University for the good quality of the ^{11}B ion beam. This work was supported by the Polish State Committee for Scientific Research, scientific and technological projects with Ukraine nos. 1243/R00/R03 and 2689/R01/R03, and Ukrainian Ministry of Education and Science. One of us (K.W. Kemper) acknowledges support of the U.S. National Science Foundation and NATO in this work.

[1] J. Cook, M. N. Stephens, and K. W. Kemper, Nucl. Phys. **A466**, 168 (1987).
[2] J. Cook, A. K. Abdallah, M. N. Stephens, and K. W. Kemper, Phys. Rev. C **35**, 126 (1987).
[3] I. J. Thompson, Comput. Phys. Rep. **7**, 167 (1988).
[4] V. K. Chernievsky *et al*., Scientific Papers of the Institute for Nuclear Research **2(8)**, 216 (2002).
[5] M. Kowalczyk, SMAN: A Code for Nuclear Experiments, Warsaw University report (1998).
[6] B. S. Nilsson, SPI-GENOA: An Optical Model Search Code, Niels Bohr Institute report (1976).
[7] A. T. Rudchik *et al*., Nucl. Phys. **A714**, 391 (2003).
[8] Yu. F. Smirnov and Yu. M. Tchuvil'sky, Phys. Rev. C **15**, 84 (1977).
[9] A. T. Rudchik and Yu. M. Tchuvil'sky, A Code DESNA, Report KIYAI-82-12 (Institute for Nuclear Research, Ukrainian Academy of Science, Kiev, 1982).
[10] A. T. Rudchik and Yu. M. Tchuvil'sky, Ukrainian Journal of Physics **30**, 819 (1985).
[11] A. N. Boyarkina, Structure of 1p-shell nuclei, Moscow State University report (1973).
[12] A. T. Rudchik *et al*., Nucl. Phys. **A695**, 51 (2001).
[13] C. Mahaux, H. Ngo, and G. R. Satchler, Nucl. Phys. **A449**, 354 (1986).
[14] A. T. Rudchik *et al*., Nucl. Phys. **A700**, 25 (2002).
[15] A. A. Rudchik *et al*., Eur. Phys. J. A **23**, 445 (2005).